

## Article

# Mechanism of Aluminum Element Segregation in As-Cast Medium-Entropy Alloy CrCoNiAl<sub>0.014</sub>: A Hybrid MD/MC Simulation and Experimental Study

Baoshuai Xue<sup>1</sup>, Zhongxue Feng<sup>1,\*</sup>, Jinliang Chen<sup>1</sup>, Chao Zhang<sup>1</sup>, Tongman Li<sup>1</sup>, Jun Tan<sup>2</sup> , Caiju Li<sup>1</sup> and Jianhong Yi<sup>1</sup>

<sup>1</sup> Faculty of Materials Science and Engineering Kunming, Kunming University of Science and Technology, Kunming 650093, China

<sup>2</sup> National Engineering Research Center for Magnesium Alloys, College of Materials Science and Engineering, Chongqing University, Chongqing 400044, China

\* Correspondence: fzxue2003@kust.edu.cn

**Abstract:** Element segregation in the as-cast medium-entropy alloy (MEA), CrCoNiAl<sub>0.014</sub>, has a significant influence on its mechanical properties. This study focused on aluminum segregation in the as-cast CrCoNiAl<sub>0.014</sub> MEA at room temperature (300 K). The element distribution, morphology, and type of precipitates formed by the elemental segregation were identified by optical microscopy, X-ray diffraction, electron probe microanalysis, and transmission electron microscopy. Al segregation existed at the dendritic boundary in the face-centered cubic (FCC) MEA matrix. Hybrid molecular dynamics and Monte Carlo simulations were conducted to analyze the diffusion behavior and the chemical affinity of Al, as well as understand the segregation mechanism of Al at the atomic scale. Al displayed a faster diffusion speed and a higher chemical affinity than Ni, Cr, and Co at the same temperature. Al segregated at the dendritic boundary to form the Al-rich phase. Furthermore, as the temperature was increased, the atomic thermal vibration of these four elements became more intensive, and Al segregation was more serious. However, Al segregation improved the uniform diffusion of Cr, Co, and Ni. Therefore, this study provides a reference for subsequent reductions in element segregation and improvements in the mechanical properties of MEA.

**Keywords:** molecular dynamics; Monte Carlo; medium-entropy alloy; element segregation



**Citation:** Xue, B.; Feng, Z.; Chen, J.; Zhang, C.; Li, T.; Tan, J.; Li, C.; Yi, J. Mechanism of Aluminum Element Segregation in As-Cast Medium-Entropy Alloy CrCoNiAl<sub>0.014</sub>: A Hybrid MD/MC Simulation and Experimental Study. *Metals* **2023**, *13*, 331. <https://doi.org/10.3390/met13020331>

Academic Editors: Changming Fang and Xiangyuan (Carl) Cui

Received: 12 December 2022

Revised: 30 January 2023

Accepted: 2 February 2023

Published: 6 February 2023



**Copyright:** © 2023 by the authors. Licensee MDPI, Basel, Switzerland. This article is an open access article distributed under the terms and conditions of the Creative Commons Attribution (CC BY) license (<https://creativecommons.org/licenses/by/4.0/>).

## 1. Introduction

Multi-primary element alloys (MPEAs) are a mixture of at least two primary elements. The proportions of constituent elements in multielement alloys are primarily equiatomic or close to equiatomic proportions. Moreover, the crystal structure of MPEAs is either a face-centered cubic (FCC) or body-centered cubic (BCC) arrangement. Nevertheless, compared to conventional alloy systems comprising one or two major elements, these MPEAs have an extraordinary structure and functional properties, which can contribute to high entropy, lattice distortion hysteresis diffusion, and stress cocktail effects in MPEAs. Therefore, these alloys have attracted extensive research interest in materials science since their introduction in 2004 [1–5]. Among MPEAs, the high-entropy alloy CrMnFeCoNi [6] and medium-entropy alloy CrCoNi [7] are used widely, exhibiting excellent high strength and high ductility at room temperature (300 K) and low temperature (77 K) [8,9]. G. Laplanc et al. [10] reported that the nanodeposition acts as an additional deformation mechanism in the medium-entropy alloy CrCoNi. Therefore, this medium-entropy alloy exhibited higher muscle strength and flexibility than the high-entropy alloy CrMnFeCoNi [10]. Zhang et al. [9] reported that the super tensile strength of the medium-entropy alloy CrCoNi was approximately 1 GPa and the failure strain was 70%. Although the medium-entropy

alloy CrCoNi has good applications in structural engineering [11–14], its yield strength at room temperature is insufficient, further limiting its extensive application in this field.

Several studies reported that adding suitable elements in high-entropy alloys (HEAs) with an FCC crystal structure could form a BCC intermetallic phase in the FCC matrix, effectively enhancing the strength-ductility synergy of HEAs [15–20]. For example, Shun [21] and Jiang [22] et al., added Mo and Nb to CrCoFeNiMo<sub>x</sub> and CrCoFeNiNb<sub>x</sub> alloys, respectively, to enhance their yield ratio. In a previous study, Al was added to the medium-entropy alloy CrCoNi to improve its yield strength. For example, Lu et al. [23] reported that when the Al content was increased gradually to 22%, the strength of the Al-containing medium-entropy alloy CrCoNi increased to 2700 Mpa, and its flexibility was 10%. Lu et al. [23] reported that adding different proportions of Al could improve the mechanical properties of Al-containing medium-entropy alloy CrCoNi. However, few studies have reported how the delayed diffusion effect of the medium-entropy alloy CrCoNiAl<sub>0.014</sub> in the as-cast status influences elemental segregation and its mechanical properties. The mechanism of element diffusion and segregation in the medium-entropy alloy CrCoNiAl<sub>0.014</sub> was established, particularly under the influence of the local chemical environment.

In addition to elemental diffusion, other factors, such as atomic radius and electronegativity, cause element segregation in the microstructure of multi-elements (e.g., medium-entropy alloy CrCoNiAl<sub>0.014</sub>). Element segregation in such alloys will indirectly affect their mechanical properties. Ding et al. [24] reported that the atomic size and electronegativity of Pd in a high-entropy alloy CoCrFeNiPd compared to the other elements (Co, Cr, Fe, and Ni) were different from those of Mn in the high-entropy alloy CoCrFeNiMn. Moreover, the element distribution of the high-entropy alloy CoCrFeNiPd was not uniform (element segregation), giving it a higher yield strength than the high-entropy alloy CoCrFeNiMn. However, under the current limited experimental means, establishing the mechanism of element diffusion and element segregation of the medium-entropy alloy CrCoNiAl<sub>0.014</sub> due to the influence of its chemical environment is challenging. The essence of element segregation in the medium-entropy alloy CrCoNiAl<sub>0.014</sub> is interatomic aggregation. Therefore, a combination of experimental and simulation methods has become the first choice to explain the atomic-level mechanism of the medium-entropy alloy CrCoNiAl<sub>0.014</sub>.

Hybrid molecular dynamics (MD) and Monte Carlo (MC) methods are used mainly to study the atomic aggregation of multielement alloys. Jian et al. [25] found that the stress of partial dislocation nucleation in medium-entropy alloy CrCoNi was increased by increasing the short-range order (SRO), which affected the yield strength of the alloy. Li et al. [26] reported that for the same system, the robustness of its energy structure could be improved by enhancing the SRO of the medium-entropy alloy CrCoNi, and the activation energy barrier can be controlled to achieve dislocation activity, thereby enhancing its strength. Furthermore, for the HEAs, CoCuFeNiPd and CoCuFeNiTi, Chen et al. [27] reported that the chemical affinity differences and exclusivity between Ti (Pd) and other elements (Co, Cu, Fe, Ni) yielded differences in chemical affinity, atomic segregation, SRO, and the agglomeration formation of these two HEAs. Hence, this method can be used to study the effects of the diffusion intensity and chemical affinity of elements on atomic segregation. However, only limited studies have been conducted on the mechanism of element segregation in medium-upper-entropy alloys using the hybrid MD/MC method. Therefore, using this hybrid simulation method to explain the influence mechanism of elemental diffusion and chemical affinity of the medium-entropy alloy CrCoNiAl<sub>0.014</sub> on its mechanical properties is of immense significance for guiding MEA processing and improving the performance design.

Optical microscopy (OM), X-ray diffraction (XRD), electron probe microanalysis (EPMA), and transmission electron microscopy (TEM) were used to examine element segregation at the dendrite grain boundary of the microstructure of the as-cast entropy alloy CrCoNiAl<sub>0.014</sub>, which is caused mainly by the segregation of the Al. Moreover, no other new phase was generated. The MD and MC simulations were combined to explore the influence of the diffusion strength of various elements (Cr, Co, Ni, and Al) and their

chemical affinity on element segregation in a medium-entropy alloy CrCoNiAl<sub>0.014</sub>. The simulations showed that the diffusivity and chemical affinity of different elements of the medium-entropy alloy CrCoNiAl<sub>0.014</sub> affect its element segregation and mechanical properties.

## 2. Method

### 2.1. Experiments

CrCoNiAl<sub>0.014</sub> ingots (30 g) were produced by melting mixtures of pure Cr (99.95%), Co (99.99%), Ni (99.99%), and Al (99.99%) in a water-cooled copper crucible under an argon atmosphere. These mixtures were remelted at least 5–6 times to achieve a uniform chemical composition. The chemical composition of the ingots was tested by inductively coupled plasma–atomic emission spectrometry (ICP–AES, Spectral Products, Windham, CT, USA), as illustrated in Table 1. Phase identification was performed by XRD (D/max-2200, Rigaku Corporation, Austin, TX, USA) using Cu–K $\alpha$  radiation at 40 kV/30 mA and a scanning step from 20° to 100° 2 $\theta$ . Metallographic and EPMA specimens of the as-cast medium-entropy alloy CrCoNiAl<sub>0.014</sub> were obtained by electropolishing using ethanol and sulfuric acid. The morphology and microstructure of the as-cast sample were characterized using a metallographic microscope and scanning electron microscope equipped with a tungsten filament and energy spectrum analyzer. The foil samples were observed by TEM (FEI TECNAI G2 F20, Thermo Fisher Scientific Inc., Waltham, Massachusetts, USA) operating at 200 keV. The TEM samples of the as-cast specimens were obtained by sequential grinding, polishing, and ion thinning.

**Table 1.** Chemical composition of CrCoNiAl<sub>0.014</sub> alloy. (at.%).

Elements	Ni	Cr	Co	Al
CrCoNiAl <sub>0.014</sub>	32.96	34.58	32.45	0.014

### 2.2. Simulation Method

The mechanism of element segregation in the microstructure of the medium-entropy alloy CrCoNiAl<sub>0.014</sub> ingot was examined. A hybrid MD/MC scheme was used to simulate its segregation behavior in the LAMMPS software package [28]. A set of embedded atom model interatomic potential functions for the Fe–Ni–Cr–Co–Al HEAs developed by Diana Franks et al. [29] was used. These potential functions could be used to predict the relative stability of the FCC-structured pentad mixture and the Al-containing phases, and verification and application of these potential functions were conducted in several studies [30–36]. The Voronoi tessellation method was adopted to establish an idealized FCC structure of the Ni polycrystalline atomic model with a lattice spacing of 3.56 Å using the Atomsk platform [37] and a large box size of 10.68 nm × 10.68 nm × 10.68 nm, which consists of more than 100,000 atoms and only 10 randomly oriented grains. Certain atoms in the Ni polycrystalline model were then replaced with Cr, Co, and Al atoms using the random substitution method, and their atomic proportions were 0.3458, 0.3245, and 0.00014, respectively. At 300 K and 700 K, a variance-constrained semi-regular ensemble was used for the MC simulation [38]. The exchange between different atoms in MC simulation follows the principle of Metropolis exchange [38]. The conventional methods were applied under the canonical ensemble MC method to calculate the chemical potential difference between Ni and Cr and Co and Al in the medium-entropy alloy CrCoNiAl<sub>0.014</sub>. Previous studies [25,39,40] calculated the difference in chemical potential between the different elements in an MPEA by combining the MC method with a semi-canonical ensemble. However, these methods must go through multiple iterations to obtain the chemical potential difference between the elements in an MPEA. To reduce the calculation cost, Campos et al. [41] proposed a new method to solve the aforementioned problem. Therefore, the chemical potential difference between Ni and Cr and Co and Al in the medium-entropy alloy CrCoNiAl<sub>0.014</sub> at 300 K and 700 K was calculated using the aforementioned new method as follows:  $\Delta\mu_{\text{Ni-Al}} = -0.902446$  eV,  $\Delta\mu_{\text{Ni-Cr}} = -0.230166$  eV,  $\Delta\mu_{\text{Ni-Co}} = -0.0395478$  eV;  $\Delta\mu_{\text{Ni-Al}} = -0.687905$  eV,

$\Delta\mu_{\text{Ni-Cr}} = -0.687905$  eV,  $\Delta\mu_{\text{Ni-Co}} = -0.0395478$  eV. The target concentrations of these four elements were  $C_{\text{Ni}} = 0.3296$ ,  $C_{\text{Cr}} = 0.3458$ ,  $C_{\text{Co}} = 0.3245$ , and  $C_{\text{Al}} = 0.00014$ , respectively. Some other specific parameters were obtained from Sadigh et al. [38]. The MD algorithm was added to the MC simulation to accelerate the convergence at the Nose–Hoover temperature under pressure control. Moreover, isothermal relaxation was performed at zero pressure with a total number of 1.2 million steps. Subsequently, the conjugate gradient method was used to eliminate the internal stress of the polycrystalline atomic model. Finally, the simulation was run for 1.2 million steps at a timestep of 1 fs tau. Periodic boundary conditions were applied to the whole simulation process.

The atomic models of 300 K and 700 K obtained via hybrid MD/MC were used to calculate the mean square displacement and the mean square displacement of the medium-entropy alloy  $\text{CrCoNiAl}_{0.014}$ . First, the atomic model was relaxed by 1 million steps at 300 K and 700 K in the NPT ensemble. Subsequently, the conjugate gradient was used to minimize its energy. Finally, the mean square displacements of each element of the medium-entropy alloy  $\text{CrCoNiAl}_{0.014}$  were calculated at 300 k and 700 k by balancing 1 million steps under the NPT ensemble again. The simulated timestep used for calculating the mean square displacement was 1 fs.

### 2.3. Post-Process

All visualization and post-treatment of the medium-entropy alloy  $\text{CrCoNiAl}_{0.014}$  were performed using the OVITO [42] package (Figure 1). The reference formulae for calculating the atomic square displacement and diffusion coefficient of the atomic model are displayed below. The formulae for calculating the internal and normalized internal accumulation energy were derived from the formulae proposed by Chen et al. [27].

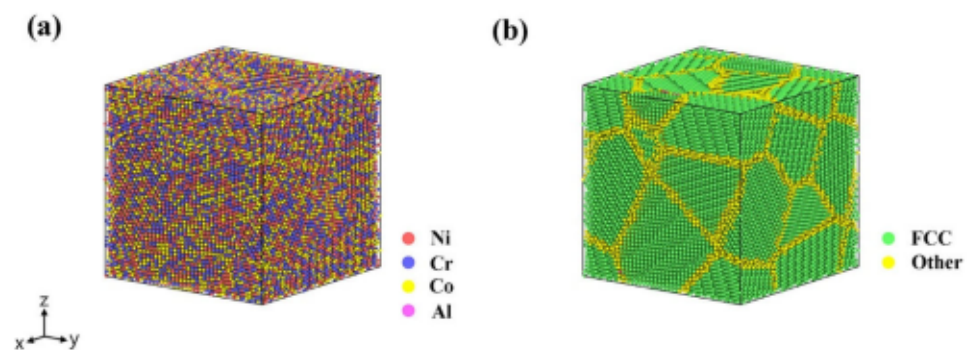


**Figure 1.** Polycrystalline atom model (a) of medium-entropy alloy  $\text{CrCoNiAl}_{0.014}$  and structure identification (b) using Common neighbor analysis module in OVITO.

The relationship between the mean square displacement ( $MSD$ ) and the time “ $t$ ” is expressed as follows:

$$MSD = R^2(t) = \frac{1}{N} \sum_{i=1}^N |x_i(t) - x_i(0)|^2 \quad (1)$$

where  $R^2(t)$  represents the average value of the atomic  $MSD$ ,  $N$  refers to the total number of atoms in the atomic model,  $x_i(t)$  indicates the position of the atom at time “ $t$ ”, and  $x_i(0)$  denotes the initial position of the atom.

The relationship between  $D$  and  $MSD$  is expressed as follows:

$$D_t = \frac{1}{6} \frac{d}{dt} \langle |r_i(t) - r_i(0)|^2 \rangle \quad (2)$$

where  $r_i(t)$  represents the  $MSD$  of the atom at time  $t$  in simulation,  $r_i(0)$  denotes the  $MSD$  of the atom at time 0 in simulation, and  $D_t$  indicates the diffusion coefficient.

The combination of cohesive energy and chemical affinity of two different elements AB (Cr, Co, Ni, and Al) of as-cast medium-entropy alloy CrCoNiAl<sub>0.014</sub> in the MD + MC simulation was characterized. The cohesive energy is expressed as follows:

$$E_c(AB) = \frac{1}{2} \{E_g(A) + E_g(B) - E_g(AB)\} \quad (3)$$

where  $E_g(AB)$  is the energy of the fully relaxed AB structure, whereas  $E_g(A)$  and  $E_g(B)$  are the energies of isolated A and B atoms in their ground state, respectively.

The normalized cohesive energy was expressed as follows:

$$E_n(AB) = [E_h - E_c(AB)] / (E_h - E_l) \quad (4)$$

where  $E_c(AB)$  denotes the cohesive energy of the AB unit cell determined by the interatomic potential,  $E_h$  is the maximum value of  $E_c(AB)$ , and  $E_l$  refers to the minimum value of  $E_c(AB)$ .

The chemical affinity (CA) is defined as:

$$C(A)(AB) = [E_n(AB) + E_n(BA)] / 2 \quad (5)$$

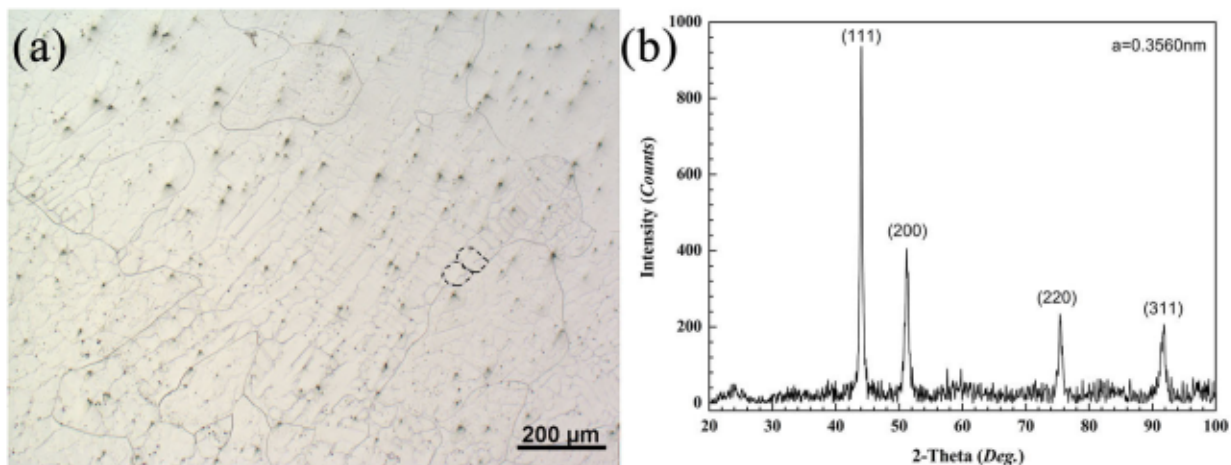
where  $E_n(AB)$  and  $E_n(BA)$  are the normalized cohesive energies of the AB and BA unit cells, respectively.

### 3. Results and Discussion

#### 3.1. Experimental

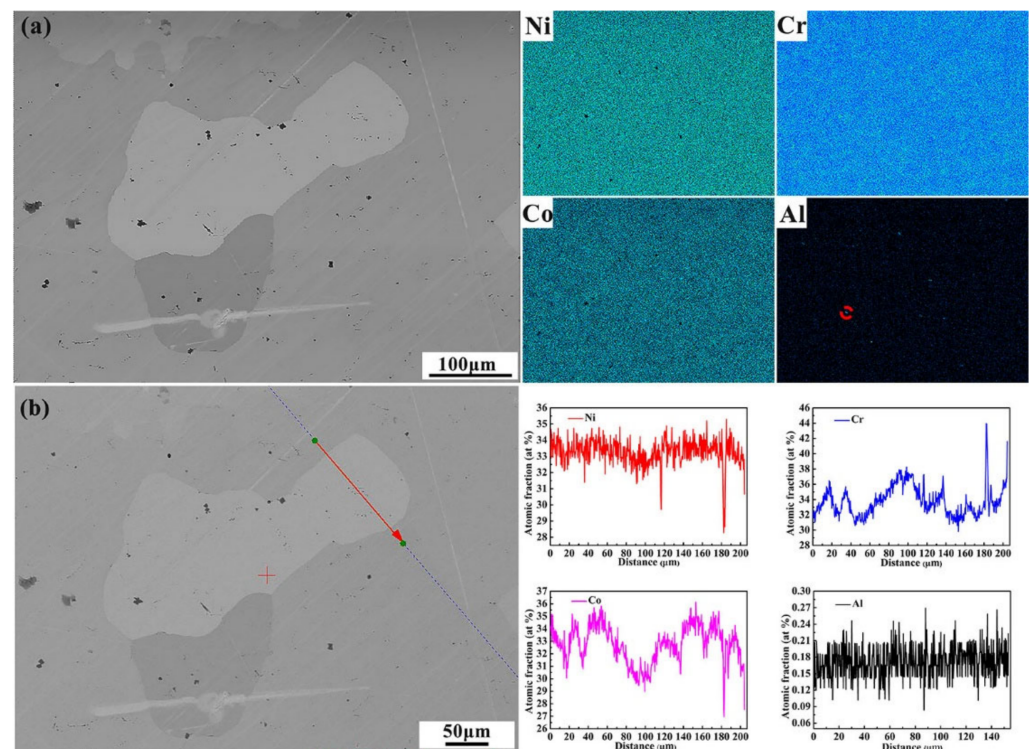
##### Microstructure and Phase Structure

Figure 2a,b show the microstructure and the XRD pattern of the as-cast medium-entropy alloy CrCoNiAl<sub>0.014</sub>, respectively. As shown in Figure 2a, the microstructure of the as-cast medium-entropy alloy CrCoNiAl<sub>0.014</sub> was composed of a cellular crystal (marked with a black dot circle), and several fine black particles were distributed at the interface of cellular crystals owing to element segregation. However, identifying them by XRD (Figure 2b) was difficult because the amount of these fine black particles was low. As a typical MEA, the matrix of the as-cast Cr-CoNiAl<sub>0.014</sub> alloy is a single-phase solid solution with an FCC crystal structure. Figure 2b shows the crystal plane index and the crystal spacing. The crystal spacing was approximately 0.356 nm. Lu et al. [21] detected a weak (111)<sub>BCC</sub> peak near the (111)<sub>FCC</sub> peak when the Al content was increased to 12%. These results showed that the elements were segregated in the microstructure of the medium-entropy alloy CrCoNiAl<sub>0.014</sub>, without forming a new segregation phase.



**Figure 2.** Microstructure (a) and the X-ray diffraction (XRD) patterns (b) of the CrCoNiAl<sub>0.014</sub> alloy.

Figure 3a,b show the surface scanning and line scanning results of Ni, Cr, Co, and Al of the as-cast medium-entropy alloy  $\text{CrCoNiAl}_{0.014}$ , detected via EPMA, respectively. Ni, Cr, and Co of the as-cast medium-entropy alloy  $\text{CrCoNiAl}_{0.014}$  are distributed uniformly, as shown in Figure 3a. However, there was a small amount of Al segregation (marked by the dotted red circle). Figure 3b shows that the fluctuation range of atomic concentrations of Ni, Cr, Co, and Al in the as-cast entropic alloy  $\text{CrCoNiAl}_{0.014}$  was 33.5, 33.5, 32.9, and 0.1 at. %, respectively. The distribution of a small amount of Al was also detected by line scanning. The composition of the wire-scanning surface of the cast medium-entropy alloy  $\text{CrCoNiAl}_{0.014}$  determined by EPMA is consistent with the quantitative composition detected via ICP–AES.



**Figure 3.** Surface scanning (a) and line scanning (b) of Ni, Cr, Co, and Al in the as-cast medium-entropy alloy  $\text{CrCoNiAl}_{0.014}$  detected by electron probe microanalysis (EPMA). The red arrow in Figure (b) shows the direction of the line scanning surface.

To determine the crystal structure of the black phase of the medium-entropy alloy  $\text{CrCoNiAl}_{0.014}$ , its microstructure and electron diffraction pattern were analyzed via TEM. The results are shown in Figure 4.

The representative TEM images of the medium-entropy alloy  $\text{CrCoNiAl}_{0.014}$  are shown in Figure 4a–c. The matrix of intermediate entropy alloy  $\text{CrCoNiAl}_{0.014}$  has no diffraction points except the diffraction points of FCC lattice (Figure 4a–c), which is consistent with the absence of a secondary phase. This result was consistent with the aforementioned XRD results. Lu et al. [21] reported that when the Al content was increased to >12%, the microstructure of the Al-containing medium-entropy alloy  $\text{CrCoNi}$  was primarily the FCC crystal structure, accompanied by a small amount of the BCC structure. Thus, the results of the present study and those reported by Lu et al. [21] validate each other.

### 3.2. Simulation

#### 3.2.1. Simulation of the Element Segregation Process

The element segregation, distribution of the Al at the grain boundary, and atomic crystal concentration of each element of the entropy alloy  $\text{CrCoNiAl}_{0.014}$  in the as-cast state were simulated by MD and MC methods, as shown in Figures 5 and 6, and Tables 2 and 3.

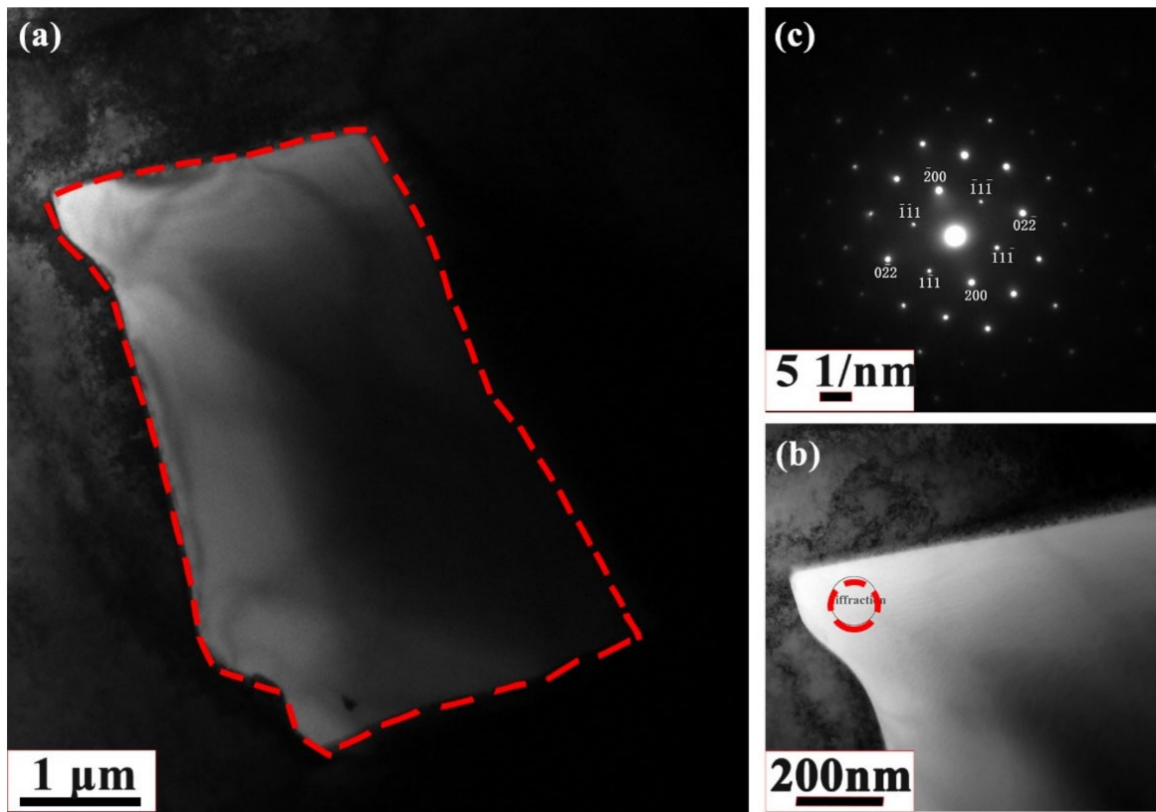


**Figure 4.** Representative TEM images of the medium entropy alloy  $\text{CrCoNiAl}_{0.014}$  under one pass rolling: (a) Transmission electron microscopy (TEM), (b) Partial enlarged image, and (c) Electron diffraction pattern of the [011] crystal plane from the selected area highlighted by the dashed circle in (b).

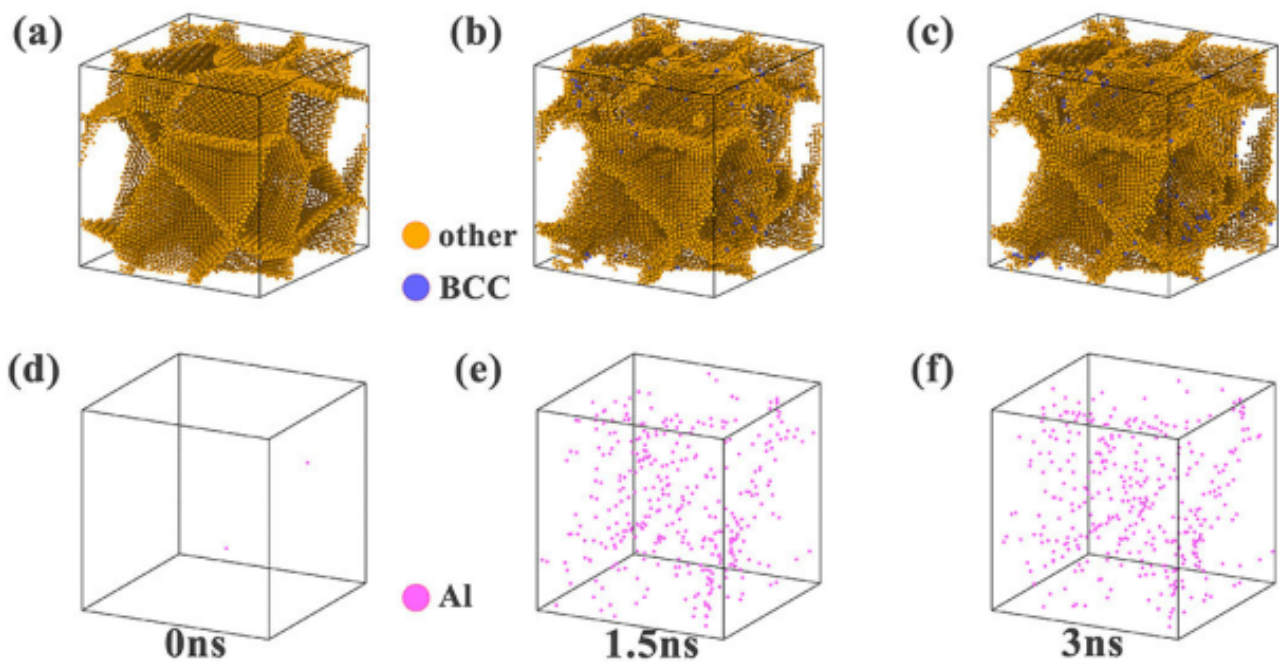


**Figure 5.** Element segregation process (a–c) and Distribution of Al elements (d–f) of the  $\text{CrCoNiAl}_{0.014}$  alloy with medium-entropy at 0, 1.5 and 3 ns grain boundaries, respectively, at 300 K.

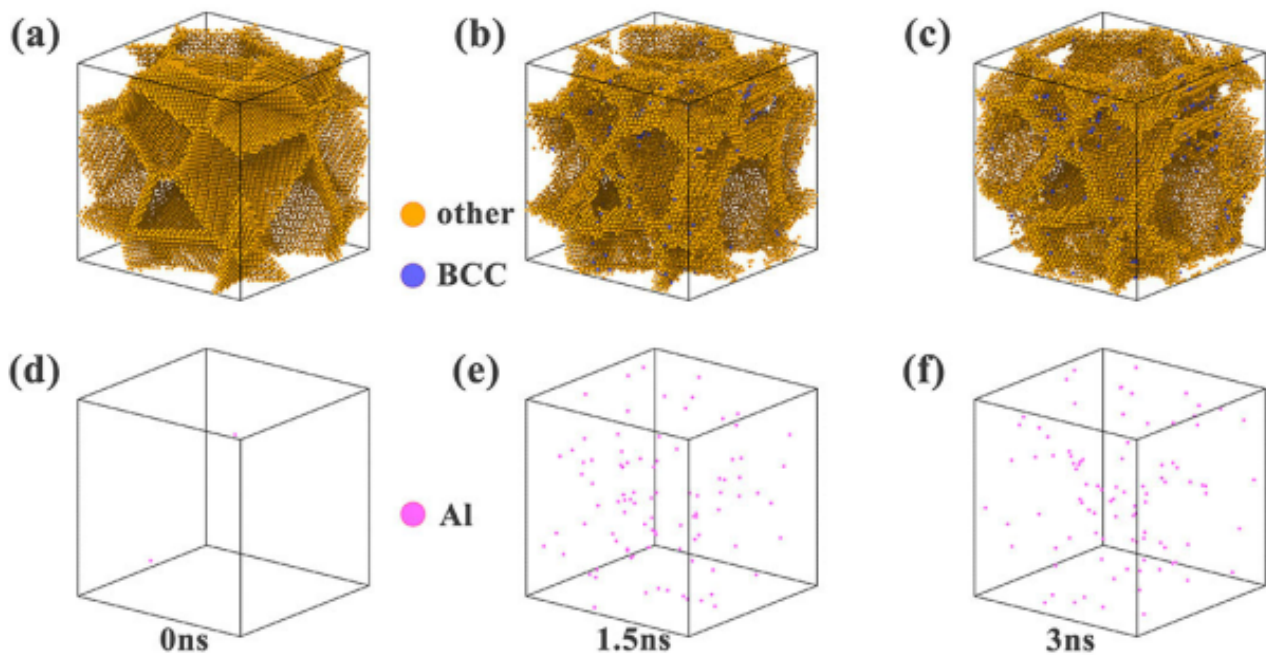


**Figure 6.** Element segregation process (a–c) and Distribution of Al elements (d–f) of the CrCoNiAl<sub>0.014</sub> alloy with medium-entropy at 0, 1.5, and 3 ns grain boundaries, respectively, at 700 K.

**Table 2.** Atomic Concentrations of Ni, Cr, Co, and Al at Grain Boundary of the Medium-Entropy Alloy CrCoNiAl<sub>0.014</sub> at 300 K.

Time (ns)	Element Concentration (at. %)			
	Cr	Co	Ni	Al
0	34.7	32.3	33.1	0.0
1.5	52.5	31.2	15.1	1.2
3	52.5	31.4	14.7	1.3

**Table 3.** Atomic Concentrations of Ni, Cr, Co, and Al at Grain Boundary of Medium-Entropy Alloy CrCoNiAl<sub>0.014</sub> at 700 K.

Time (ns)	Element Concentration (at. %)			
	Cr	Co	Cr	Al
0	34.7	32.3	33.1	0.0
1.5	42.5	31.6	25.5	0.3
3	42.3	31.7	25.7	0.3

Figures 5a–f and 6a–f present the atomic segregation process of the grain boundary surface and the distribution of Al at the grain boundary of the medium-entropy alloy CrCoNiAl<sub>0.014</sub> at 0, 1.5, and 3 ns at 300 and 700 K, respectively. At 300 K and 700 K, the grain boundary of polycrystalline CrCoNiAl<sub>0.014</sub> was observed at 0 ns (Figures 5a–c and 6a–c); no atoms from other structures were detected on the grain boundary surface. This result was because a perfect crystal structure is maintained by the initial polycrystalline model established at the initial stage. As the overall energy of the polycrystalline model tends to be stable, a few atoms within the BCC structure appear on the grain boundary surface of the polycrystalline model CrCoNiAl<sub>0.014</sub>. The atoms of the BCC structure on the grain boundary surface existed as a single atom and did not form atomic clusters. This is because under the influence of the thermal vibration of the atom, with decreasing overall energy, the diffusion rate of the medium-entropy alloy CrCoNiAl<sub>0.014</sub> containing the trace Al at

the grain boundary is greater than that in the crystal. The concentration of Al at the grain boundaries of medium-entropy alloy CrCoNiAl<sub>0.014</sub> was higher at 300 K than at 700 K (Figure 5e,f and Figure 6e,f). The formation of the BCC crystal structure on the grain boundary surface of the medium-entropy alloy CrCoNiAl<sub>0.014</sub> is related to the increase in the concentration of Al at the grain boundary.

The changes in the atomic concentration of other elements at the grain boundary of the medium-entropy alloy CrCoNiAl<sub>0.014</sub> were examined. Tables 2 and 3 lists the changes in the atomic concentration of each element at the grain boundary of the medium-entropy alloy CrCoNiAl<sub>0.014</sub> at 300 and 700 K, respectively. The atomic concentrations of the Ni and Co decrease at the grain boundaries of the medium-entropy alloy CrCoNiAl<sub>0.014</sub>. In contrast, the atomic concentrations of Cr and Al increased at the grain boundaries at 300 K and 700 K, respectively, from 0 to 1.5 ns. From 1.5 to 3 ns, no change in the atomic concentrations of Ni, Cr, Co, and Al at the grain boundaries was observed.

### 3.2.2. Atomic Trajectories and Element Diffusion

The simulations of the abovementioned medium-entropy alloy CrCoNiAl<sub>0.014</sub> show that the single BCC crystal structure formed via grain boundary segregation is related to its chemical environment. In particular, the single BCC crystal structure is related to the diffusion of the elements of the alloy. Figure 7a,b and Figure 8a–d show the atomic trajectory, MSD, and diffusion rate of the medium-entropy alloy CrCoNiAl<sub>0.014</sub> at 300 and 700 K, respectively.

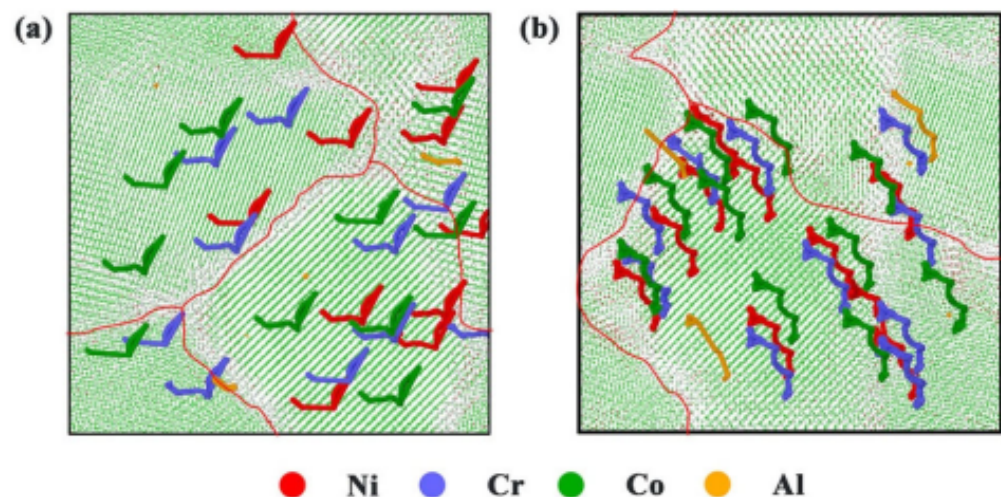


**Figure 7.** Atomic diffusion trajectory of medium-entropy alloy CrCoNiAl<sub>0.014</sub> at annealing temperatures of 300K (a) and 700K (b).

A slice of atoms normal to  $x$ , the [100] direction, was selected for visualization with a cut-off distance of 30 angstroms ( $\text{\AA}$ ) to trace the atomic trajectory in the element diffusion process of medium-entropy alloy CrCoNiAl<sub>0.014</sub>. Therefore, atomic trajectories of the medium-entropy alloy CrCoNiAl<sub>0.014</sub> represents the operation of projecting a three-dimensional diffusion pattern on the  $yz$  plane. Figure 7a shows that Ni, Cr, Co, and Al of the medium-entropy alloy CrCoNiAl<sub>0.014</sub> escape from the initial position at 300 K and travel a certain distance in the crystal, suggesting that diffusion occurs at an MD time of 4.2 ns. Compared with the tuple diffusion track of each element of the medium-entropy alloy CrCoNiAl<sub>0.014</sub> at 300 K, significant improvement was observed in the cumulative diffusion displacement of Al at 700 K compared to that of Ni, Cr, and Co (Figure 7b). Hence, with increasing temperature, Al becomes more active in dynamics than Ni, Cr, and Co. In addition, at 300 K and 700 K, the atomic trajectory lines of Ni, Cr, Co, and Al had a herringbone shape because the element diffusion is not controlled along a specific vacancy, and the overall diffusion trajectory occurs randomly with the vibration of the lattice.

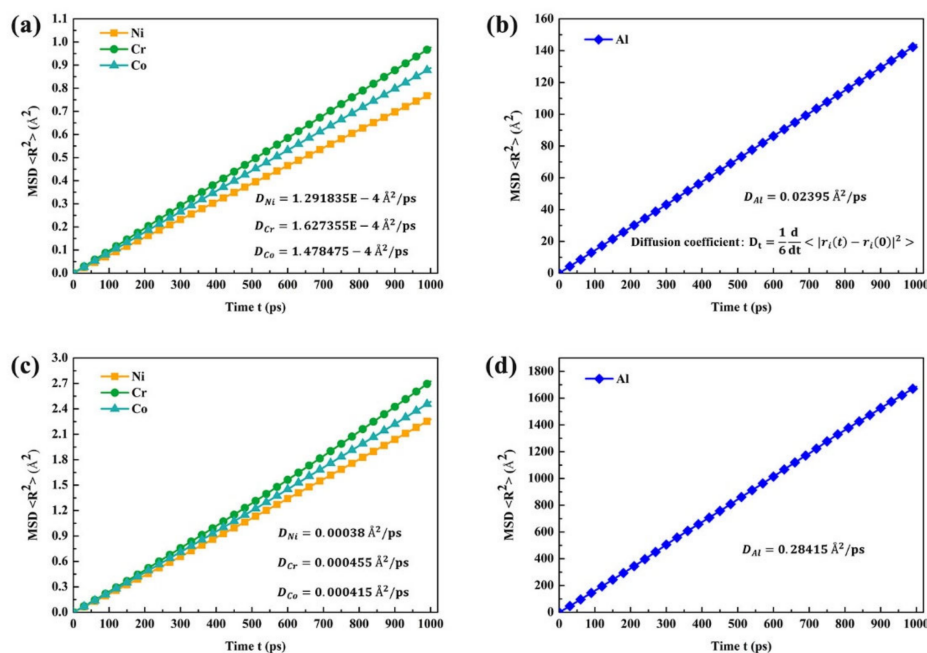


**Figure 8.** Mean square displacement and diffusion rate (a,c) of Ni, Cr, and Co elements, and mean square displacement and diffusion rate (b,d) of Al elements of the medium-entropy alloy  $\text{CrCoNiAl}_{0.014}$  at 300 and 700 K.

The relationship between  $MSD$  and time change at 300 and 700 K and the fitted diffusion rate was simulated to quantify the dynamic inhomogeneity of element diffusion in the medium-entropy alloy  $\text{CrCoNiAl}_{0.014}$ , as illustrated in Figure 8a–d, respectively. Figure 8a–d shows that the  $MSD$  of the Ni, Cr, Co, and Al in the medium-entropy alloy  $\text{CrCoNiAl}_{0.014}$  increases with temperature. The  $MSD$  of the Al atoms increased faster than that of Ni, Cr, and Co atoms. However, at 300 and 700 K, the  $MSD$  of Al in the medium-entropy alloy  $\text{CrCoNiAl}_{0.014}$  was the highest, whereas that of Ni was the lowest. This phenomenon showed that the Al becomes more active than Ni, Cr, and Co with increasing temperature, which is consistent with the comparison of atomic trajectories in Figure 8a,b. The formula in Figure 8b was used for fitting and calculating the diffusion rate of each element in the medium-entropy alloy  $\text{CrCoNiAl}_{0.014}$ . The fitting results showed that the diffusion rate of the Al is higher than that of Ni, Cr, and Co.

### 3.2.3. Cohesive Energy and Chemical Affinity

From the MD perspective, this study revealed the relationship between the element segregation process and the element diffusion of the medium-entropy alloy  $\text{CrCoNiAl}_{0.014}$ . The process of element segregation is affected by the diffusion of elements and is constrained by the force between the elements, particularly the chemical affinity. Therefore, the cohesive energy and chemical affinity in the  $\text{CrCoNiAl}_{0.014}$  atomic model are demonstrated as follows:

Figure 9a,b show the cohesion energy and CA of the atomic model of the medium-entropy alloy  $\text{CrCoNiAl}_{0.014}$ . The cohesive energy between the Ni–Ni (Cr, Co) in the  $\text{CrCoNiAl}_{0.014}$  atomic model was greater than  $-4$  eV (Figure 9a); the cohesive energy between Al–Ni (Cr, Co) was between  $-3$  and  $4$  eV, and the cohesive energy between the Al–Al parts was less than  $-3$  eV. Therefore, Al–Al in  $\text{CrCoNiAl}_{0.014}$  belonged to high-energy clusters. Al–Ni (Cr, Co) belonged to medium-energy groups, and Ni–Ni (Cr, Co) belonged to low-energy clusters. The cohesive energy of Al–Al (Ni, Cr, and Co) in  $\text{CrCoNiAl}_{0.014}$  is greater than that of Ni–Ni (Cr, Co). Among them, the cohesive energy of Al–Al was the largest, with the cohesive energy of Ni–Ni being the smallest. The CA between Ni–Ni (Cr, Co) in the  $\text{CrCoNiAl}_{0.014}$  atomic model was  $>0.8$  (Figure 9b). This CA was double the  $0.28$ – $0.35$  observed between Al–Ni (Cr, Co). The affinity between Al–Al was 0. However,

the CA of Al–Al (Ni, Cr, and Co) was smaller than that of Ni–Ni (Cr, Co). Among them, the CA between Al–Al was the largest. According to the inherent law of the cohesive energy and CA between Ni–Ni (Al, Cr, and Co) in the CrCoNiAl<sub>0.014</sub> atomic model, with Ni–Ni, Cr–Cr, Co–Co, and Al–Al is the same. The greater the cohesive energy between different Ni–Cr (Al, Co) indicated a weaker CA between the medium-entropy alloy CrCoNiAl<sub>0.014</sub> components (Ni, Cr, Co, and Al).

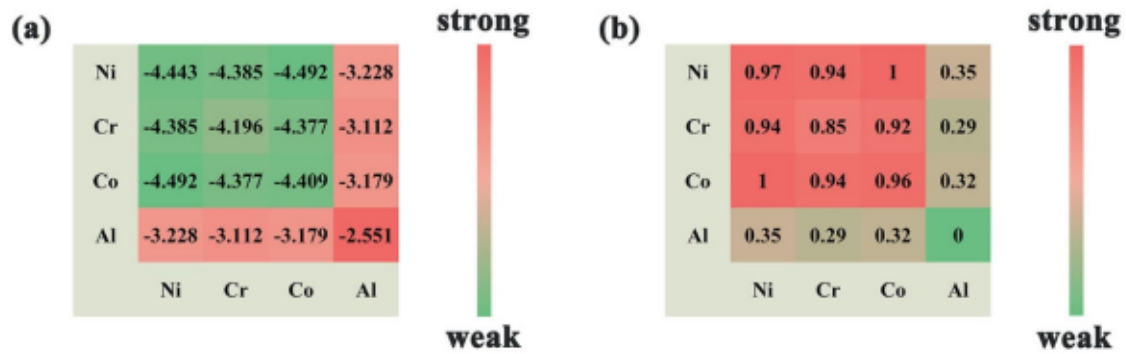


**Figure 9.** Cohesive energy (a) and chemical affinity (b) of CrCoNiAl<sub>0.014</sub> based upon the MD data (Units in Figure 4a: eV).

Hybrid MD and MC simulations showed that Al–Al (Ni, Cr, and Co), i.e., the CrCoNiAl<sub>0.014</sub> atomic model species, belonged to high-energy clusters, and their CA was relatively low compared to that excluding Al bonding. Along with the binding energy (cohesive energy) between the atoms, the constraints of the binding force between the atoms also exist. When the temperature was increased from 300 to 700 K, the atomic thermal vibration frequency of CrCoNiAl<sub>0.014</sub> increased. The nuclear bonding force between Al–Al was considerably weaker than that of Cr–Cr (Co–Co and Ni–Ni). Therefore, Cr, Co, Ni, and Al were diffused. The activation energy of diffusion required to form Al–Al was considerably weaker than that between Cr–Cr (Co–Co and Ni–Ni). Hence, the rate of Al diffusion was higher than that of Cr, Co, and Ni. Finally, a small amount of Al was transferred from the inner region of the grain to the grain boundary. When the energy trend of the whole CrCoNiAl<sub>0.014</sub> element system is stable, a few atoms in the form of BCC clusters gather on the grain boundary surface.

Mixed MD and MC simulations showed that the segregation of the parts is distinctly impacted by the diffusion speed of the solid-solution alloy elements and the strength of their CA. However, in the context of the unbalanced crystallization of the as-cast medium-entropy alloy CrCoNiAl<sub>0.014</sub>, the degree of microstructure segregation was affected by the cooling rate, element diffusion, and other factors. Finally, the simulations provided a better solution for the subsequent solution to the element segregation problem of the medium-entropy alloy CrCoNiAl<sub>0.014</sub>.

#### 4. Conclusions

The experiment results and mechanism of element segregation of the medium-entropy alloy CrCoNiAl<sub>0.014</sub> were studied through MD + MC simulations and experiments. The studies led to the following conclusions:

- (1) Element segregation at the dendrite boundary was demonstrated by the metallographic microstructure of the as-cast medium-entropy alloy CrCoNiAl<sub>0.014</sub>. Aluminum segregation resulted mainly in dendrite grain boundary segregation of the as-cast medium-entropy alloy CrCoNiAl<sub>0.014</sub>, and no other new phase was generated.
- (2) The hybrid MD and MC method showed that atomic segregation occurred at the grain boundaries of CrCoNiAl<sub>0.014</sub> polycrystals owing to the CA and diffusivity between Al–Al. With the prolonged holding time, a small amount of Al can transfer to the grain boundary in the CrCoNiAl<sub>0.014</sub> polycrystal.

- (3) Based on the element segregation rule of the cast entropy alloy CrCoNiAl<sub>0.014</sub>, the hybrid MD and MC methods, a comprehensive explanation was provided concerning the simulation results and influencing factors of the element segregation of the as-cast entropy alloy CrCoNiAl<sub>0.014</sub>. In the process of its unbalanced crystallization, although the as-cast entropy alloy CrCoNiAl<sub>0.014</sub> with regard to the diffusion rate and CA of Cr, Co, Ni, and Al would cause element segregation in the microstructure, these elements could also be affected by other factors, such as the cooling rate. The MD simulation considered the influence of other factors on the element segregation of the medium-entropy alloy CrCoNiAl<sub>0.014</sub>, which is the future scope of this study. Therefore, the combination of MD and MC simulation with the element segregation experiment of the as-cast entropy alloy CrCoNiAl<sub>0.014</sub> provided a reference for the subsequent improvement in the mechanical properties of the as-cast entropy alloy CrCoNiAl<sub>0.014</sub> in the as-cast state.

**Author Contributions:** B.X.: Conceptualization, Methodology, Software, Validation, Investigation, Writing—Original draft, Writing—Review and Editing, Visualization. Z.F.: Conceptualization, Writing—Original draft, Writing—Review and Editing, Visualization, Supervision, Funding acquisition, Project administration. J.C.: Conceptualization, Methodology, Validation, Investigation, Writing—Original draft, Writing—Review and Editing, Visualization. C.Z.: Conceptualization, Methodology, Writing—Review and Editing, Visualization. T.L.: Conceptualization, Supervision, Project administration. J.T.: Conceptualization, Supervision, Project administration. C.L.: Supervision, Project administration. J.Y.: Supervision, Project administration. All authors have read and agreed to the published version of the manuscript.

**Funding:** This work was supported by Yunnan Major Scientific and Technological Projects (grant NO. 202202AG050004), the general project of Yunnan Provincial Science and Technology Department (NO. 202001AT070041), the National Natural Science Foundation of China (No. 51861016), Chongqing Tongliang District Surface Project, TL00-5, and Henan Key Laboratory of Material Science and Technology (MDE2019-04).

**Institutional Review Board Statement:** Not applicable.

**Informed Consent Statement:** Informed consent was obtained from all subjects involved in the study.

**Data Availability Statement:** Not applicable.

**Conflicts of Interest:** The authors declare that they have no known competing financial interest or personal relationships that could have appeared to influence the work reported in this paper.

## References

1. Cantor, B.; Chang, I.T.H.; Knight, P.; Vincent, A.J.B. Microstructural development in equiatomic multicomponent alloys. *Mater. Sci. Eng. A* **2004**, *375–377*, 213–218. [[CrossRef](#)]
2. Cury, F.G.; Zepon, G.; Bolfarini, C. Multi-principal element alloys from the CrCoNi family: Outlook and perspectives. *J. Mater. Res. Technol.* **2021**, *15*, 3461–3480. [[CrossRef](#)]
3. George, E.P.; Curtin, W.; Tazan, C. High entropy alloys: A focused review of mechanical properties and deformation mechanisms. *Acta Mater.* **2020**, *188*, 435–474. [[CrossRef](#)]
4. Miracle, D.B.; Senkov, O.N. A critical review of high entropy alloys and related concepts. *Acta Mater.* **2017**, *122*, 448–511. [[CrossRef](#)]
5. Ye, Y.F.; Wang, Q.; Lu, J.; Liu, C.; Yang, Y. High-entropy alloy: Challenges and prospects. *Mater. Today* **2016**, *19*, 349–362. [[CrossRef](#)]
6. Wu, Z.; Bei, H.; Otto, F.; Pharr, G.; George, E. Recovery, recrystallization, grain growth and phase stability of a family of FCC-structured multi-component equiatomic solid solution alloys. *Intermetallics* **2014**, *46*, 131–140. [[CrossRef](#)]
7. Gludovatz, B.; Hohenwarter, A.; Catoor, D.; Chang, E.H.; George, E.P.; Ritchie, R.O. A fracture-resistant high-entropy alloy for cryogenic applications. *Science* **2014**, *345*, 1153–1158. [[CrossRef](#)]
8. Gludovatz, B.; Hohenwarter, A.; Thurston, K.V.S.; Bei, H.; Wu, Z.; George, E.P.; Ritchie, R.O. Exceptional damage-tolerance of a medium-entropy alloy CrCoNi at cryogenic temperatures. *Nat. Commun.* **2016**, *7*, 10602. [[CrossRef](#)]
9. Zhang, Z.; Sheng, H.; Wang, Z.; Gludovatz, B.; Zhang, Z.; George, E.P.; Yu, Q.; Mao, S.X.; Ritchie, R.O. Dislocation mechanisms and 3D twin architectures generate exceptional strength-ductility-toughness combination in CrCoNi medium-entropy alloy. *Nat. Commun.* **2017**, *8*, 14390. [[CrossRef](#)]
10. Laplanche, G.; Kostka, A.; Reinhart, C.; Hunfeld, J.; Eggeler, G.; George, E.P. Reasons for the superior mechanical properties of medium-entropy CrCoNi compared to high-entropy CrMnFeCoNi. *Acta Mater.* **2017**, *128*, 292–303. [[CrossRef](#)]

11. Tsai, K.-Y.; Tsai, M.-H.; Yeh, J.-W. Sluggish diffusion in Co–Cr–Fe–Mn–Ni high-entropy alloys. *Acta Mater.* **2013**, *61*, 4887–4897. [[CrossRef](#)]
12. Yeh, J.-W. Alloy design strategies and future trends in high-entropy alloys. *JOM* **2013**, *65*, 1759–1771. [[CrossRef](#)]
13. Miracle, D.B.; Miller, J.D.; Senkov, O.N.; Woodward, C.; Uchic, M.D.; Tiley, J. Exploration and development of high entropy alloys for structural applications. *Entropy* **2014**, *16*, 494–525. [[CrossRef](#)]
14. Lim, K.R.; Lee, K.S.; Lee, J.S.; Kim, J.Y.; Chang, H.J.; Na, Y.S. Dual-phase high-entropy alloys for high-temperature structural applications. *J. Alloys Compd.* **2017**, *728*, 1235–1238. [[CrossRef](#)]
15. Zhang, M.; Zhou, X.; Li, J. Microstructure and mechanical properties of a refractory CoCrMoNbTi high-entropy alloy. *J. Mater. Eng. Perform.* **2017**, *26*, 3657–3665. [[CrossRef](#)]
16. Huo, W.; Zhou, H.; Fang, F.; Zhou, X.; Xie, Z.; Jiang, J. Microstructure and properties of novel CoCrFeNiTax eutectic high-entropy alloys. *J. Alloys Compd.* **2018**, *735*, 897–904. [[CrossRef](#)]
17. Yang, Q.; Tang, Y.; Wen, Y.; Zhang, Q.; Deng, D.; Nai, X. Microstructures and properties of CoCrCuFeNiMox high-entropy alloys fabricated by mechanical alloying and spark plasma sintering. *Powder Met.* **2017**, *61*, 115–122. [[CrossRef](#)]
18. Tan, Y.; Li, J.; Wang, J.; Kolbe, M.; Kou, H. Microstructure characterization of CoCrFeNiMnPd eutectic high-entropy alloys. *J. Alloys Compd.* **2018**, *731*, 600–611. [[CrossRef](#)]
19. Jiang, H.; Han, K.; Qiao, D.; Lu, Y.; Cao, Z.; Li, T. Effects of Ta addition on the microstructures and mechanical properties of CoCrFeNi high entropy alloy. *Mater. Chem. Phys.* **2018**, *210*, 43–48. [[CrossRef](#)]
20. Gao, X.; Lu, Y.; Zhang, B.; Liang, N.; Wu, G.; Sha, G.; Liu, J.; Zhao, Y. Microstructural origins of high strength and high ductility in an AlCoCrFeNi2.1 eutectic high-entropy alloy. *Acta Mater.* **2017**, *141*, 59–66. [[CrossRef](#)]
21. Shun, T.-T.; Chang, L.-Y.; Shiu, M.-H. Microstructure and mechanical properties of multiprincipal component CoCrFeNiMox alloys. *Mater. Charact.* **2012**, *70*, 63–67. [[CrossRef](#)]
22. Jiang, H.; Jiang, L.; Qiao, D.; Lu, Y.; Wang, T.; Cao, Z.; Li, T. Effect of niobium on microstructure and properties of the CoCrFeNb<sub>x</sub> Ni high entropy alloys. *J. Mater. Sci. Technol.* **2017**, *33*, 712–717. [[CrossRef](#)]
23. Lu, W.; Luo, X.; Yang, Y.; Zhang, J.; Huang, B. Effects of Al addition on structural evolution and mechanical properties of the CrCoNi medium-entropy alloy. *Mater. Chem. Phys.* **2019**, *238*, 121841. [[CrossRef](#)]
24. Ding, Q.; Zhang, Y.; Chen, X.; Fu, X.; Chen, D.; Chen, S.; Gu, L.; Wei, F.; Bei, H.; Gao, Y.; et al. Tuning element distribution, structure and properties by composition in high-entropy alloys. *Nature* **2019**, *574*, 223–227. [[CrossRef](#)]
25. Jian, W.-R.; Xie, Z.; Xu, S.; Su, Y.; Yao, X.; Beyerlein, I.J. Effects of lattice distortion and chemical short-range order on the mechanisms of deformation in medium entropy alloy CoCrNi. *Acta Mater.* **2020**, *199*, 352–369. [[CrossRef](#)]
26. Li, Q.-J.; Sheng, H.; Ma, E. Strengthening in multi-principal element alloys with local-chemical-order roughened dislocation pathways. *Nat. Commun.* **2019**, *10*, 3563. [[CrossRef](#)]
27. Chen, S.; Aitken, Z.H.; Pattamatta, S.; Wu, Z.; Yu, Z.G.; Banerjee, R.; Srolovitz, D.J.; Liaw, P.K.; Zhang, Y.-W. Chemical-affinity disparity and exclusivity drive atomic segregation, short-range ordering, and cluster formation in high-entropy alloys. *Acta Mater.* **2021**, *206*, 116638. [[CrossRef](#)]
28. Plimpton, S. Fast parallel algorithms for short-range molecular dynamics. *J. Comput. Phys.* **1995**, *117*, 1–19. [[CrossRef](#)]
29. Farkas, D.; Caro, A. Model interatomic potentials for Fe–Ni–Cr–Co–Al high-entropy alloys. *J. Mater. Res.* **2020**, *35*, 3031–3040. [[CrossRef](#)]
30. Jarlöv, A.; Ji, W.; Zhu, Z.; Tian, Y.; Babicheva, R.; An, R.; Seet, H.L.; Nai, M.L.S.; Zhou, K. Molecular dynamics study on the strengthening mechanisms of Cr–Fe–Co–Ni high-entropy alloys based on the generalized stacking fault energy. *J. Alloys Compd.* **2022**, *905*, 164137. [[CrossRef](#)]
31. Li, J.; Yang, X.; Wang, P.; An, Q. Dynamic interactions between low-angle grain boundary and stacking fault tetrahedron in Ni-Fe solid solution alloys. *J. Alloys Compd.* **2022**, *907*, 164572. [[CrossRef](#)]
32. Al Hasan, M.A.; Wang, J.; Shin, S.; Gilbert, D.A.; Liaw, P.K.; Tang, N.; Liyanage, W.N.C.; Santodonato, L.; DeBeer-Schmitt, L.; Butch, N.P. Effects of aluminum content on thermoelectric performance of Al CoCrFeNi high-entropy alloys. *J. Alloys Compd.* **2022**, *883*, 160811. [[CrossRef](#)]
33. Lu, Y.-S.; Chang, M.-P.; Fang, T.-H. Phase transformation and microstructure evolution of nanoimprinted NiCoCr medium entropy alloys. *J. Alloys Compd.* **2022**, *892*, 162138. [[CrossRef](#)]
34. Sun, Z.; Shi, C.; Gao, L.; Lin, S.; Li, W. Thermal physical properties of high entropy alloy Al<sub>0.3</sub>CoCrFeNi at elevated temperatures. *J. Alloys Compd.* **2022**, *901*, 163554. [[CrossRef](#)]
35. Zhang, N.; Gan, K.; Li, Z. Atomistic insights on the deformation mechanisms of Cox(CrNi)<sub>100-x</sub> multicomponent alloys: The effect of Co content. *Comput. Mater. Sci.* **2022**, *211*, 111559. [[CrossRef](#)]
36. Abere, M.J.; Ziade, E.; Lu, P.; Saltonstall, C.B.; Gu, X.; Wright, W.J.; Argibay, N.; Kustas, A.B. A predictive analytical model of thermal conductivity for aluminum/transition metal high-entropy alloys. *Scr. Mater.* **2022**, *208*, 114330. [[CrossRef](#)]
37. Hirel, P. Atomsk: A tool for manipulating and converting atomic data files. *Comput. Phys. Commun.* **2015**, *197*, 212–219. [[CrossRef](#)]
38. Sadigh, B.; Erhart, P.; Stukowski, A.; Caro, A.; Martinez, E.; Zepeda-Ruiz, L. Scalable parallel Monte Carlo algorithm for atomistic simulations of precipitation in alloys. *Phys. Rev. B* **2012**, *85*, 184203. [[CrossRef](#)]
39. Utt, D.; Stukowski, A.; Albe, K. Grain boundary structure and mobility in high-entropy alloys: A comparative molecular dynamics study on a Σ11 symmetrical tilt grain boundary in face-centered cubic CuNiCoFe. *Acta Mater.* **2019**, *186*, 11–19. [[CrossRef](#)]

40. Ma, S.; Zhang, J.; Xu, B.; Xiong, Y.; Shao, W.; Zhao, S. Chemical short-range ordering regulated dislocation cross slip in high-entropy alloys. *J. Alloys Compd.* **2022**, *911*, 165144. [[CrossRef](#)]
41. Campos, R.P.; Shinzato, S.; Ishii, A.; Nakamura, S.; Ogata, S. Database-driven semigrand canonical Monte Carlo method: Application to segregation isotherm on defects in alloys. *Phys. Rev. E* **2021**, *104*, 025310. [[CrossRef](#)] [[PubMed](#)]
42. Stukowski, A. Visualization and analysis of atomistic simulation data with OVITO—The Open Visualization Tool. *Model. Simul. Mater. Sci. Eng.* **2010**, *18*, 015012. [[CrossRef](#)]

**Disclaimer/Publisher’s Note:** The statements, opinions and data contained in all publications are solely those of the individual author(s) and contributor(s) and not of MDPI and/or the editor(s). MDPI and/or the editor(s) disclaim responsibility for any injury to people or property resulting from any ideas, methods, instructions or products referred to in the content.